2nd Advanced Optical Metrology Compendium

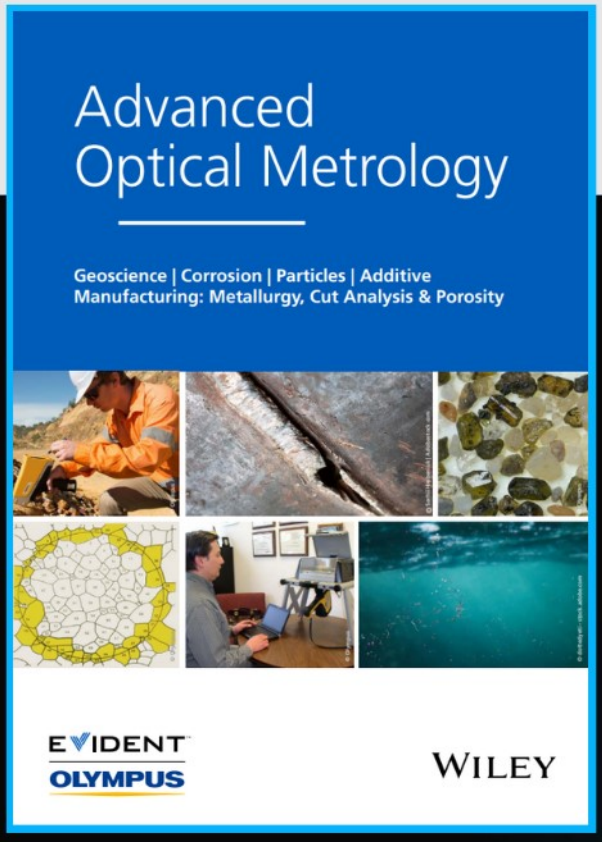

The latest eBook from Advanced Optical Metrology. Download for free.

This compendium includes a collection of optical metrology papers, a repository of teaching materials, and instructions on how to publish scientific achievements.

With the aim of improving communication between fundamental research and industrial applications in the field of optical metrology we have collected and organized existing information and made it more accessible and useful for researchers and practitioners.

EVIDENT
OLYMPUS

WILEY

ADVANCED FUNCTIONAL MATERIALS
www.afm-journal.de

Complementary Surface-Enhanced Raman Scattering (SERS) and IR Absorption Spectroscopy (SEIRAS) with Nanorods-on-a-Mirror

Eitan Oksenberg, Ilan Shlesinger, Gökçen Tek, A. Femius Koenderink, and Erik C. Garnett**

The surface-enhanced counterparts of Raman scattering (SERS) and infrared (IR) absorption (SEIRAS) are commonly used to probe and identify nanoscale matter and small populations of molecules. The contrasting selection rules offer complementary vibrational information of bulk solids or solutions. In this study, a complementary surface-enhanced vibrational spectroscopy approach is presented to probe the vibrational signature of metal-bound molecular monolayers. Nanocavities are designed and produced with sharp and tunable visible (VIS) and mid-IR gap resonances by placing nanorods on a mirror that is coated with a thin dielectric spacer. Their VIS resonances are tuned to match a 1.61 eV (770 nm) resonant excitation for SERS, while their mid-IR resonances span the 1500–2800 cm^{-1} range (6.5–3.5 µm) in high resolution for SEIRAS, targeting CN bond vibrations at 2220 cm^{-1}. Both the VIS and mid-IR gap modes support spatially overlapping and highly enhanced near-fields ensuring strong SERS and SEIRAS signals from the same monolayer molecular population. The differences in the vibrational information obtained with the two surface-enhanced spectroscopies when probing coupled molecular vibrations are highlighted and the advantages of using such a platform for investigating cavity-modified chemical reactions are discussed.

1. Introduction

Vibrational spectroscopy provides a nondestructive and label-free approach to identify substances.[1] As such, it is widely used to detect and identify molecules, pollutants, or impurities, and monitor processes in a wide variety of industrial and basic research fields including chemistry, biology, materials science, physics, food, pharma, and forensics.[2–7] The vibrational signature of a chemical bond can be probed through the absorption of mid-infrared (IR) light or Raman scattering of, predominantly, visible (VIS) light. Owing to the different underlying physical processes, the corresponding spectroscopies have complementary selection rules. IR absorption spectroscopy can be used to detect vibrations that alter the dipole moment of the bond (IR active modes) while symmetric vibrations that alter the polarizability of the molecular bond can be seen through Raman spectroscopy (Raman active modes).[1] Together, IR and Raman spectroscopy provide complementary information over the full vibrational fingerprint of a given substance.

For decades, the extremely low cross sections of both IR absorption and Raman scattering (roughly 10^{-20} and 10^{-30} cm^{-2}, respectively) have severely limited their use in sensing applications to mostly bulk liquids or solids. These limitations have been gradually lifted following the discovery and development of surface-enhanced Raman scattering (SERS) during the 1970s and surface-enhanced IR absorption spectroscopy (SEIRAS) in the 1980s.[8–10] The greatly enhanced IR absorption and Raman scattering cross sections in close proximity to metallic structures have expanded the applicability of vibrational spectroscopy to increasingly reduced amounts of material. Driven by the advances in nanoscience during the last decades, single-molecule SERS is now a relatively common and established practice,[11] while SEIRAS is slightly lagging with detection limits that approach a few hundred molecules.[12] These differences stem primarily from the fundamental differences between SERS and SEIRAS. In the nonlinear Raman scattering process, the enhanced electromagnetic field intensity impacts both the excitation and radiation efficiency generating an electromagnetic enhancement (G_{SERS}) that scales as $|E(\omega)/E_0(\omega)|^2_{ext}|E(\omega)/E_0(\omega)|^2_{rad}$.[11] In SEIRAS the electromagnetic enhancement (G_{SEIRAS}) simply scales with the enhanced field intensity $|E(\omega)/E_0(\omega)|^2$. Beyond this fundamental difference, focusing mid-IR light into small volumes through nanophotonic design for SEIRAS has proven more challenging than obtaining highly enhanced fields in the VIS for SERS.

E. Oksenberg, I. Shlesinger, G. Tek, A. F. Koenderink, E. C. Garnett
AMOLF
Science Park 104, Amsterdam 1098 XG, The Netherlands
E-mail: E.Oksenberg@amolf.nl; e.c.garnett@uva.nl
E. C. Garnett
Institute of Physics
University of Amsterdam
Science Park 904, Amsterdam 1098 XH, The Netherlands
The ORCID identification number(s) for the author(s) of this article can be found under https://doi.org/10.1002/adfm.202211154.

DOI: 10.1002/adfm.202211154

Arguably, the greatest field enhancement and localization, and the corresponding strongest surface-enhanced vibrational signals, can be obtained using nanoscale to picoscale gaps between metallic structures.[12–15] The nanoparticle-on-a-mirror (NPoM) construct gives rise to sharp VIS resonances and extremely enhanced and localized fields in the small gap between a nanoparticle and a mirror substrate.[13] These plasmonic constructs have been successfully used, amongst others, to track chemical processes,[16] control radiative processes,[17] and investigate single-molecule strong coupling at room temperature.[18] One practical advantage of NPoMs is the relative ease and reproducibility of fabrication. NPoMs can be produced simply by drop casting nanoparticles on a metallic mirror covered with a self-assembled monolayer (SAM) of molecules, a polyelectrolyte molecular spacer or a thin dielectric layer deposited using atomic layer deposition (ALD).[13] In most mid-IR cavities, on the other hand, the photonic structures that funnel mid-IR light into small gaps have been prepared using top-down nanofabrication approaches that limit the reproducibility and size of the nanogaps.[12,14] Furthermore, to collect the long mid-IR wavelengths, mostly large photonic structures are used (usually not smaller than a few micrometers).[12,14,19–21] The size of these cavities would likely be a limiting factor in larger-scale signal optimization as it determines the maximal number of cavities per area.

An optimal platform for complementary SERS and SEIRAS should provide spatially overlapping and highly enhanced fields in the VIS and mid-IR range. These two requirements ensure strong spectroscopic signals from the same molecular population. Additionally, narrow and easily tunable mid-IR resonances are advantageous for probing or coupling specific bond vibrations. Demonstrations of nanophotonic platforms that support both SERS and SEIRAS have been very limited.[22–25] They involve either 2D or 3D arrays of fabricated,[24] or self-assembled,[22,23,25] nanostructures with nanoscale gaps. Impressive SERS and SEIRAS signals have been reported using these systems, yet each poses drawback. More specifically, D'Andrea et al. used nanorod arrays that are resonant in both the visible (short axis excitation) and the mid-IR (long axis excitation).[24] By selecting the wavelength and polarization of the excitation, they generate mid-IR or VIS resonances for SEIRAS or SERS. However, their system lacks the necessary spatial overlap of the VIS and mid-IR resonant modes for complementary spectroscopy on the same molecular population. Furthermore, The VIS resonances provide only a mild field enhancement ($E/E_0 = 4$) while the stronger mid-IR resonances ($E/E_0 = 141$) show broad linewidths. On the other hand, 2D (Le et al.)[23] or 3D (Mueller et.al.)[25] nanoparticle arrays show good spatial overlap using a broadband approach providing only mild enhanced fields ($E/E_0 \approx 10–20$) in both spectral ranges.

Here, we present a complementary surface-enhanced vibrational spectroscopy approach for obtaining strong SERS and SEIRA signals from the same monolayer molecular population using nanorods-on-a-mirror (NRoM) nanocavities (**Figure 1**a). The geometric anisotropy of the nanorods gives rise to resonances at very different spectral ranges. The formed NRoM construct provides sharp resonances in the VIS (short-axis excitation) and mid-IR (long-axis excitation) that can be easily tuned across a large spectral range by varying the gap size, either by changing the thickness of the spacer or by varying the width (VIS resonance) or length (mid-IR resonance) of the nanorods. The NRoMs show exceptionally high enhanced and localized fields in both the VIS ($E/E_0 = 110$), and mid-IR ($E/E_0 = 230$) with a high degree of spatial overlap (≈77%). We design and fabricate NRoMs with VIS gap resonances that match the 1.61 eV (770) nm laser we use for SERS. At the same time, the mid-IR resonances are tailored to span, in high resolution, the 1500–2800 cm^{-1} (6.5–3.5 μm) range targeting the CN bond vibration (≈2220 cm^{-1}). With strong and complementary SERS and SEIRAS signals gathered from a thiol self-assembled monolayer (SAM) and NRoMs arrays, we demonstrate the versatility and potency of the dual optical range nanocavity. Focusing on the vibrational signature of weakly coupled CN vibrations, we highlight the differences in the obtained vibrational information using SERS and SEIRAS, and discuss the advantages of using NRoMs when investigating how VIS or mid-IR cavities can modify chemical reactions.

2. Results and Discussion

2.1. Simulations

The dual-range NRoM nanocavity consists of a gold nanorod that is separated by a thin dielectric spacer from a gold mirror, as illustrated in Figure 1a. Lumerical's finite-difference time-domain (FDTD) calculations were used to evaluate the extinction spectra of a 70 nm thick rounded-edge nanorod separated by a 6 nm Al_2O_3 layer from a flat gold mirror. Figure 1b shows the simulated extinction spectra resulting from normal incidence short-axis excitation of the (11) gap mode. By varying the width of the nanorod from 50 to 80 nm in increments of 10 nm, the VIS gap resonance is tuned across the 1.3–1.8 eV range (≈680–950 nm). This spectral range was chosen to match our experimental setup. However, the VIS gap resonance can be pushed further to higher or lower energies by using narrower or wider nanorods respectively. Upon normal incidence long-axis excitation, the simulated extinction spectra (Figure 1c) reveal sharp mid-IR resonances that correspond to the dipolar mode (1900–3100 cm^{-1}) and broader resonances at higher energies that correspond to the sextupole mode (Figure S1a, Supporting Information). By varying the length of the nanorod from 400 to 700 nm in increments of 100 nm, the mid-IR gap resonances are tuned across the 1900–3100 cm^{-1} range (5.2–3.2 μm). Tuning further the mid-IR gap resonances toward lower or higher energies can be done by using longer or shorter nanorods respectively.

Further FDTD calculations were used to extract the near-field profile of an NRoM following resonant excitation. The field profile of a 70 × 70 × 750 nm nanorod following normal incidence short-axis resonant excitation at 1.5 eV is shown in Figure 1d. As seen in the logarithmic-scale color map, the near-fields are confined to the gap between the nanorod and the mirror generating fields that are up to 110 times larger than the incoming field. The near-field profile of the NRoM construct upon long-axis resonant excitation at 2000 cm^{-1} (0.25 eV, 5 μm) can be seen in Figure 1c. As is the case for the VIS resonant excitation,

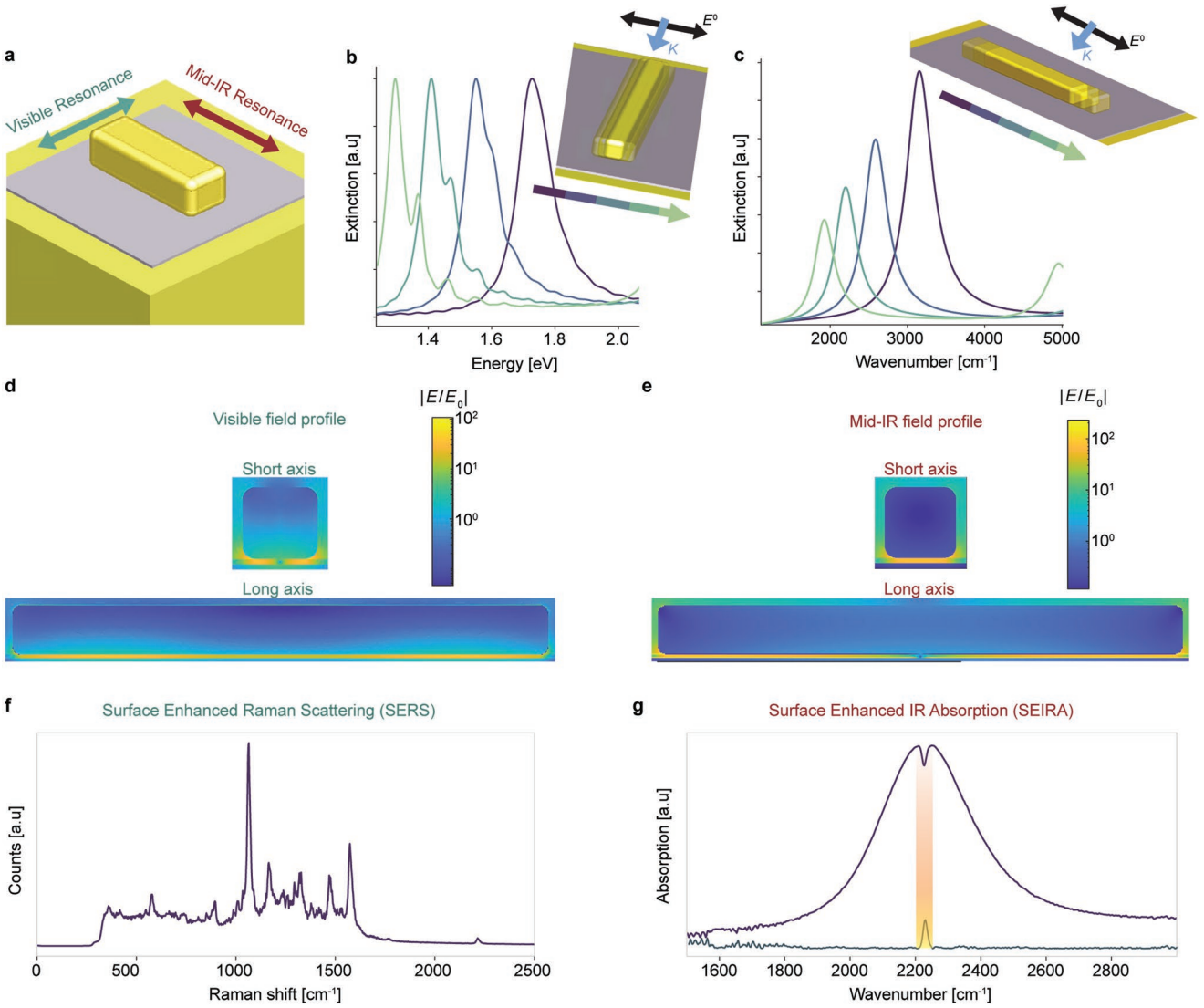

Figure 1. Nanorod-on-a-mirror (NRoM) for complementary surface-enhanced vibrational spectroscopy. a). Schematic illustration of the NRoM construct. b,c). Simulated FDTD extinction spectra for a 70 nm thick nanorod separated by a 6 nm Al_2O_3 layer from the gold mirror and normal incident excitation, E^0 and K are the electric field amplitude and wave vector of the incident light. b) Short-axis excitation gives rise to VIS gap resonances that are tuned by varying the width of the nanorod from 50 to 80 nm (purple to green). c) Long-axis excitation results in mid-IR gap resonances that are tuned by varying the length of the nanorod from 400 to 700 nm (purple to green). d,e). Simulated logarithmic-scale field-enhancement profiles of the NRoM after resonant excitation d) in the VIS (1.5 eV, short-axis excitation) and e) in the mid-IR (2000 cm^{-1}, long-axis excitation). f,g). Experimental demonstration of f) SERS and g) SEIRAS spectra of the same molecular population obtained using NRoMs (details are discussed in the following paragraphs).

the mid-IR resonant excitation also results in near-fields that are confined to the nanogap, producing fields that are up to 230 times the magnitude of the incoming field. When comparing the VIS and mid-IR near-field profiles shown in Figure 1d,e, it is apparent that the two modes are mostly spatially overlapping, with small variations in the field penetration into the nanorod (a spatial overlap map of the two modes can be found in Figure S1c–e, Supporting Information). Using a spatial overlap integral over a 2D slice in the middle of the gap, we estimate a ≈77% overlap between the two modes. This is a key feature of the NRoM cavity for complementary surface-enhanced vibrational spectroscopy as it ensures that the SERS and SEIRAS signals are generated predominantly from the same molecular population that resides within the gap and toward the nanorod edges, where the near-fields of both the VIS and mid-IR modes are maximized. Furthermore, the orientations of the field vectors of both modes are mostly orthogonal to the substrate (Figure S1f, Supporting Information), therefore, the relative orientation between the field vector and the probed bond vibration in both SERS and SEIRAS are expected to be similar. This feature is especially important when investigating well-ordered molecular assemblies such as SAMs. Experimental SERS (Figure 1f) and SEIRAS (Figure 1g) spectra are shown to illustrate the role of the VIS and mid-IR gap resonances in this complementary approach and will be discussed in detail in the following paragraphs.

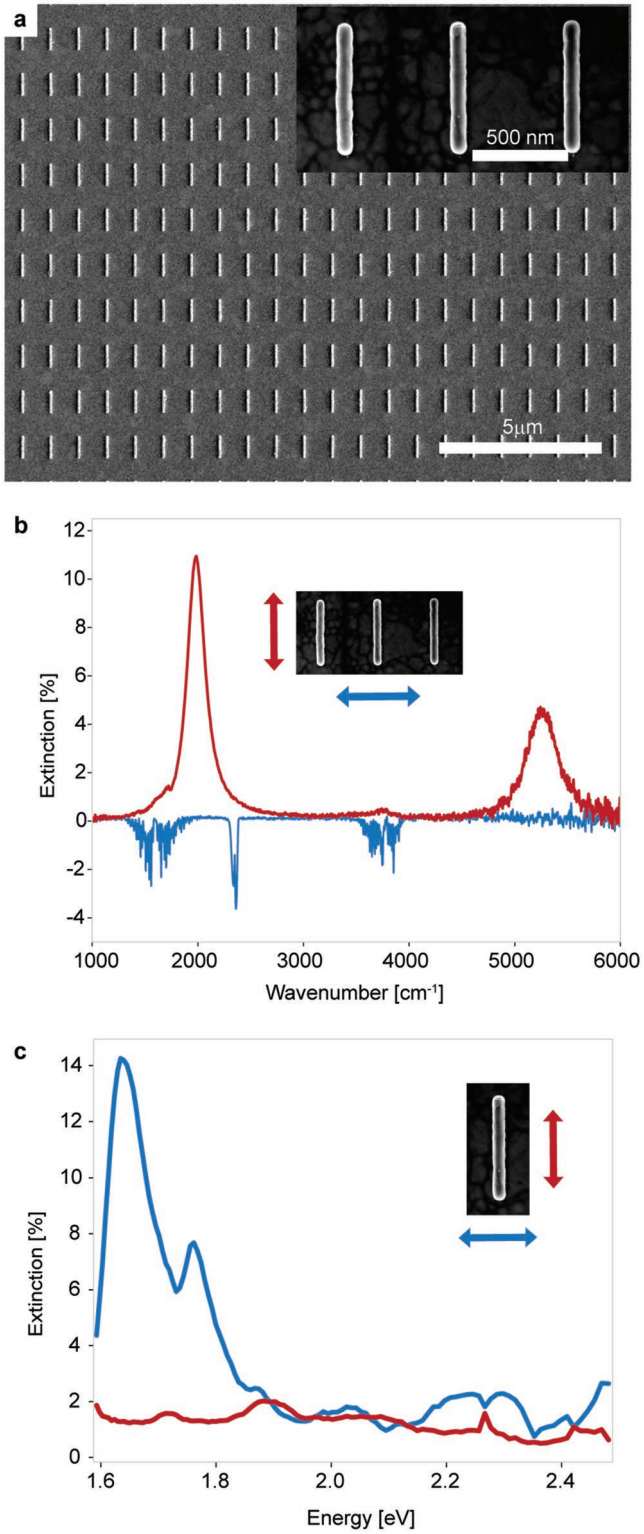

Figure 2. NRoM experimental characteristics. a) SEM image of fabricated NRoM arrays with a higher magnification image in the inset. b) Mid-IR extinction spectra of a NRoM array (nanorod dimension is $70 \times 70 \times 750$ nm) showing a polarization-dependent response. Long-axis excitation (red) induces sharp mid-IR resonances while short-axis excitation (blue) results in noise and residual water vapor and CO_2 vibrational dips. c). VIS extinction spectra also show an orthogonal response as long-axis excitation (red) results in mostly noise while short-axis excitation (blue) gives rise to a strong gap resonance ≈760 nm (1.63 eV).

2.2. Fabrication and Characterization

To realize NRoMs constructs and validate spectroscopically the simulated behavior, 100 nm thick gold mirrors were evaporated on Si substrates followed by ALD deposition of Al_2O_3 thin layers (2–4 nm). Then, arrays of nanorods 70 nm thick, 70 nm wide of varying lengths (600–800 nm, in 5 nm increments) were fabricated on another Si substrate using electron beam lithography (EBL) and gold evaporation. Next, taking advantage of the poor adhesion between the Si native oxide and gold nanorods, the nanorods were stripped from the Si substrate and transferred onto the coated gold mirrors using a thermal release tape forming the NRoMs constructs. A detailed description can be found in Experimental Section and Figure S2 (Supporting Information) along with a discussion of transfer yields and their impact on the collected data. The nanorod transfer is not strictly required to construct NRoMs, as nanorods can be fabricated directly on top of the coated gold mirrors. However, the transfer step was found to be crucial to ensure the formation of a SAM in the gap where the maximal fields reside (Figure S2, Supporting Information). Furthermore, we have successfully fabricated NRoMs using the more scalable nanocube imprint lithography approach (Figure S3, Supporting Information).[26] Single NRoM investigations, which are likely achievable using state-of-the-art FTIR microscopes, would lift the need to form arrays. In that case, single NRoMs could also be fabricated simply by drop casting colloidally synthesized nanorods onto coated mirrors and located, for example, using correlative electron and optical microscopy. Due to the higher degree of flexibility in the fabrication, for this proof-of-concept demonstration, we discuss throughout this manuscript NRoMs fabricated with EBL and gold evaporation.

A scanning electron microscopy (SEM) image of a typical NRoM array can be seen in **Figure 2**a. We characterize the arrays (nanorod dimension is $70 \times 70 \times 750$ nm) using a Fourier-transform infrared (FTIR) microscope (Bruker Hyperion coupled to a Bruker Vertex 80v spectrometer) in reflection mode through a ×15 reflective objective using a standard thermal light source and an integration time of 30–60 s. We characterize NRoM arrays, and not single cavities to compensate for the relatively low brilliance of the IR light source of our FTIR microscope. The arrays offer an improved signal to noise, while we deliberately avoid array phenomena such as surface lattice resonances. Reducing the collection area and effectively probing smaller arrays results in noisier spectra that show the same spectral features following normalization (Figure S4, Supporting Information), suggesting that the array measurements reflect the behavior of single NRoMs but with increased linewidths due to superradiant damping and inhomogeneous linewidth broadening as discussed in the next paragraph.

Typical polarization-dependent FTIR spectra of a NRoM array can be seen in Figure 2b. When excited along the long-axis (red) sharp mid-IR resonances can be clearly observed,

matching nicely with the expected spectrum from the FDTD simulations (Figure 1c). Upon short-axis excitation (blue) only noise and residual vibrational dips of water vapors and CO_2 are seen. These dips stem from instabilities in the vapor environment in our home-built nitrogen chamber that is mounted on the FTIR microscope. The full width at half maximum (FWHM) of the FTIR spectra gathered from various NRoM arrays with the same period is typically between 300–450 cm^{-1}, depending predominantly on the resonance frequency (Figure S5a,b, Supporting Information), the spacer thickness, and fabrication errors. The period of the array strongly impacts the linewidth as it determines the superradiant damping associated with arrays of subwavelength scatterers.[27] The FWHM of a simulated resonance spectrum centered at ≈2300 cm^{-1} using a single NRoM is ≈42 cm^{-1} (Figure S5, Supporting Information), while the simulated resonance spectra centered at 1900–3100 cm^{-1} (Figure 1c) using NRoM arrays with a 100 nm long axis gap between the nanorods exhibit linewidths between 310–420 cm^{-1} in nice agreement with our experimental linewidths. Experimental linewidths as low as 200 cm^{-1} were reached using metallic NRoM arrays with larger periods (Figure S5, Supporting Information), which is quite noteworthy considering possible inhomogeneous broadening due to small variation in the fabricated nanorods and the expected radiative losses associated with fairly rough evaporated gold used for both the mirrors and nanorods. Single NRoM extinction measurements using integrating sphere microscopy (see Experimental Section for details) can be seen in Figure 2c, where long-axis excitation over the VIS spectral range (red) does not show any noticeable resonances while short-axis excitation (blue) gives rise to the gap plasmon resonance, in agreement with our simulations (Figure 1b).

2.3. Complementary SERS and SEIRAS

To demonstrate the use of NRoM arrays for sensitive complementary SERS and SEIRAS, we chose to focus on the distinct and well-separated CN vibration at ≈2220 cm^{-1}. We assemble a SAM of 4-mercaptobenzonitrile (4-MBN) onto the nanorods by soaking the NRoM sample in a 10 mM solution of 4-MBN (Fluorochem) in ethanol for ≈24 h. Several functionalization protocols were tested as detailed in Experimental Section and Figure S6 (Supporting Information). After the assembly, we performed SERS measurements on a few selected single NRoMs. We take advantage of the VIS gap resonance ≈770 following short-axis excitation and conduct a polarization-dependent measurement using a 772 nm (1.61 eV, 300–900 μW μm^{-2}, 5–10 s integration) laser excitation. The polarization-dependent SERS spectra are presented in **Figure 3**a,b, revealing the vibrational signature of 4-MBN and the CN vibration ≈2220 cm^{-1} (highlighted with a dashed red line) only following short-axis excitation (Figure 3a). Long-axis excitation under the same conditions generates only the background signal. Considering only the electromagnetic enhancement of the SERS signal that scales as $|E(\omega)/E_0(\omega)|^4$ and the simulated field enhancement profiles, we set an upper bound for the SERS enhancement at $\approx|110|^4 = 1.5 \times 10^8$.

To demonstrate the complementary SEIRAS measurements targeting the CN vibration, we first measure the extinction spectra of bare NRoMs to make sure that we span the appropriate frequency range. As described earlier the sample consists of 60 fields (200 × 200 μm) with NRoM arrays. We use 70 nm thick, and 70 nm wide nanorods while varying the length in each field from 600 to 800 nm, in 5 nm increments. The obtained FTIR spectra (Figure 3c) reveal sharp mid-IR resonances that span the 2000 to 3000 cm^{-1} range in high resolution. After assembling the 4-MBN monolayer, the interaction between the mid-IR resonances and the CN bond vibration at 2220 cm^{-1} can be clearly observed (Figure 3d, dashed red line). As expected, this interaction becomes more pronounced as the detuning between the cavity resonance and the bond vibration decreases. In fact, while recording the extinction spectra of NRoMs with cavity resonances that have no overlap with the CN bond vibration, the signal from that vibration cannot be observed (**Figure 4**a, purple).

Taking a closer look at the interaction between the bond vibration and the cavity resonance, in Figure 3e, we highlight three spectra with a varying degree of detuning. To extract the vibrational information, we reconstruct the uncoupled NRoM resonance and subtract it from the coupled system to obtain background-subtracted curves (details in Experimental Section). The background-subtracted curves are presented in Figure 3f revealing Fano-type interactions indicating that the nanocavity-CN bond system is firmly in the weak coupling regime. This behavior is expected considering the differences between the linewidth of the optical resonance (typically ≈300 cm^{-1} in this frequency range) and the molecular vibration (≈13 cm^{-1}), highlighting the very different damping rates of these oscillators.[28] When the resonant frequencies of the NRoM and the bond vibration match (Figure 3e, green), the background-subtracted curve exhibits an inverted Lorentzian lineshape. The absolute value of the inverted Lorentzian is shown in Figure 3f, middle panel. It is centered at 2225 cm^{-1} with an FWHM of 13 cm^{-1} in good agreement with the expected spectroscopic signature of a CN bond vibration. When the optical resonance is at lower or higher energies (Figure 3e, purple and blue, respectively), the asymmetric Fano lineshape is seen in the background-subtracted spectra (Figure 3f, top and bottom panels, respectively) with the expected sign flip.[28] To assess the coupling strength of the system we fit the data to a coupled oscillator model and find coupling strengths of ≈20 cm^{-1} (Figure 3g; Figure S7, Supporting Information).[29] The behavior of the system was also emulated with FDTD simulations using a 2 nm shell of a Lorentz material representing an oscillator at the CN vibration frequency (Figure S7, Supporting Information).

To estimate the number of probed molecules, we consider a single NRoM and a rough assessment of the SAM surface coverage (≈5 molecules nm^{-2}).[30] The vibrational signals in SEIRAS are considered to be predominantly generated from areas with high field enhancements.[31] Taking into account the simulated field enhancement profiles (Figure 1g), we estimate a contributing area of ≈10 000–30 000 nm^2 corresponding to 50 000–150 000 molecules. Importantly, we did not determine experimentally the surface coverage or the molecular orientation of the SAM, but both parameters can dramatically impact the strength of the SEIRAS signal. In fact, we see substantially reduced signals when using the same experimental configuration and assembling a slightly different SAM, this time

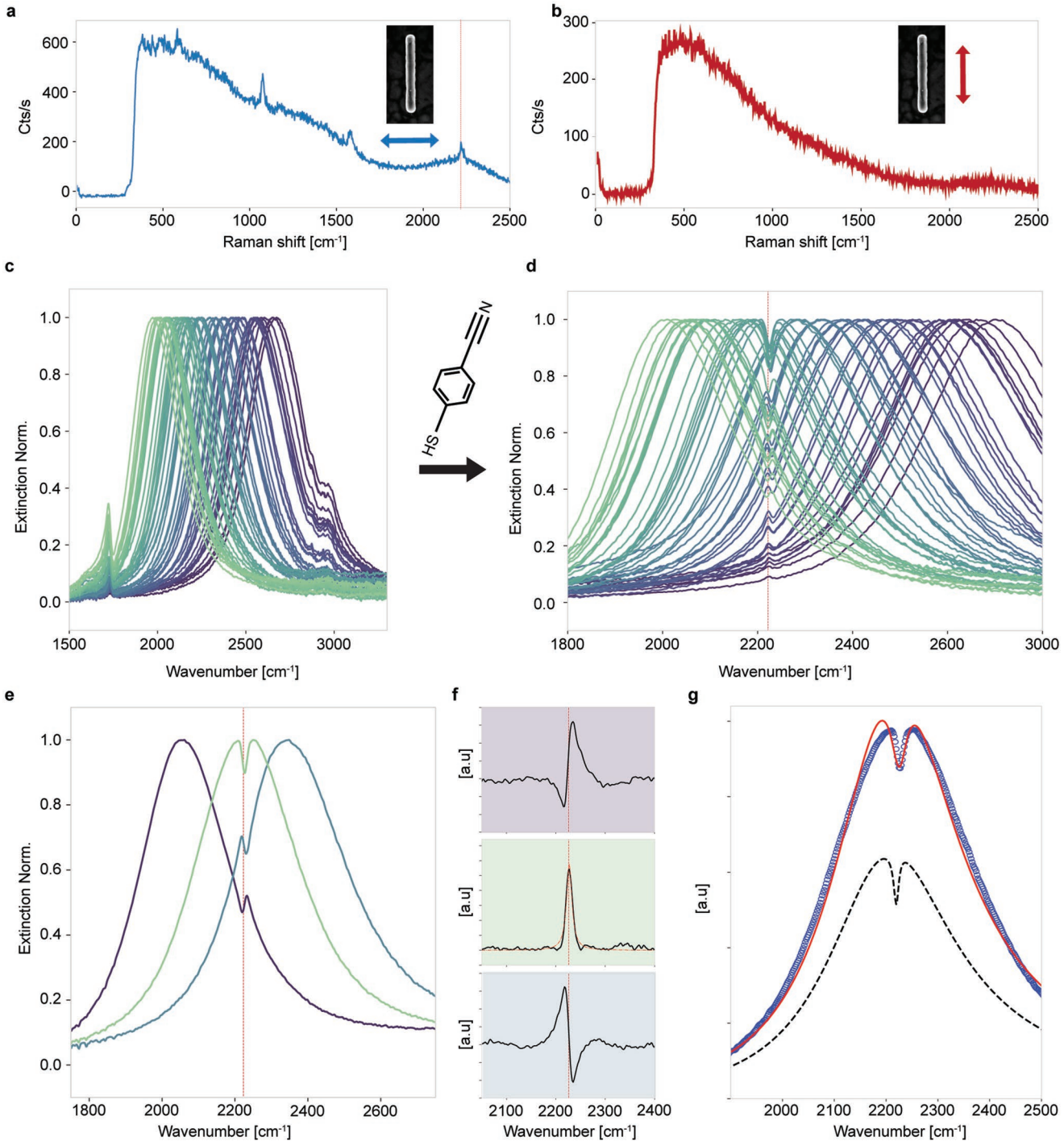

Figure 3. Complementary SERS and SEIRAS with NRMs. a,b) polarization-dependent SERS spectra taken with a 772 nm laser (1.61 eV, 360 μW μm^{-2}, 5 s integration) while exciting a) the short-axis (CN vibration highlighted with a dashed red line), and b) the long-axis of the NRoM. c). Collected FTIR spectra of bare NRoMs with varying lengths spanning the energy range of interest. d) FTIR spectra following the assembly of a 4-MBN monolayer on the nanorods. the red-dashed line highlights the expected position of the CN vibration e) FTIR spectra with a varying degree of detuning between the optical resonance and the bond vibration and f) their corresponding background-subtracted curves. g) Fitting of the matched FTIR spectrum (green) to a coupled oscillator model, showing the data (blue circles), initial guess (dashed black), and fitted curve (red).

3-mercaptobenzonitrile (Enamine), with the CN vibration in the meta position (Figure S8, Supporting Information). The reduced signals might stem from differences in the packing density of the monolayer or reduced orientational overlap between the CN dipole and the electric field vector. Considering only the electromagnetic enhancement of the SEIRAS

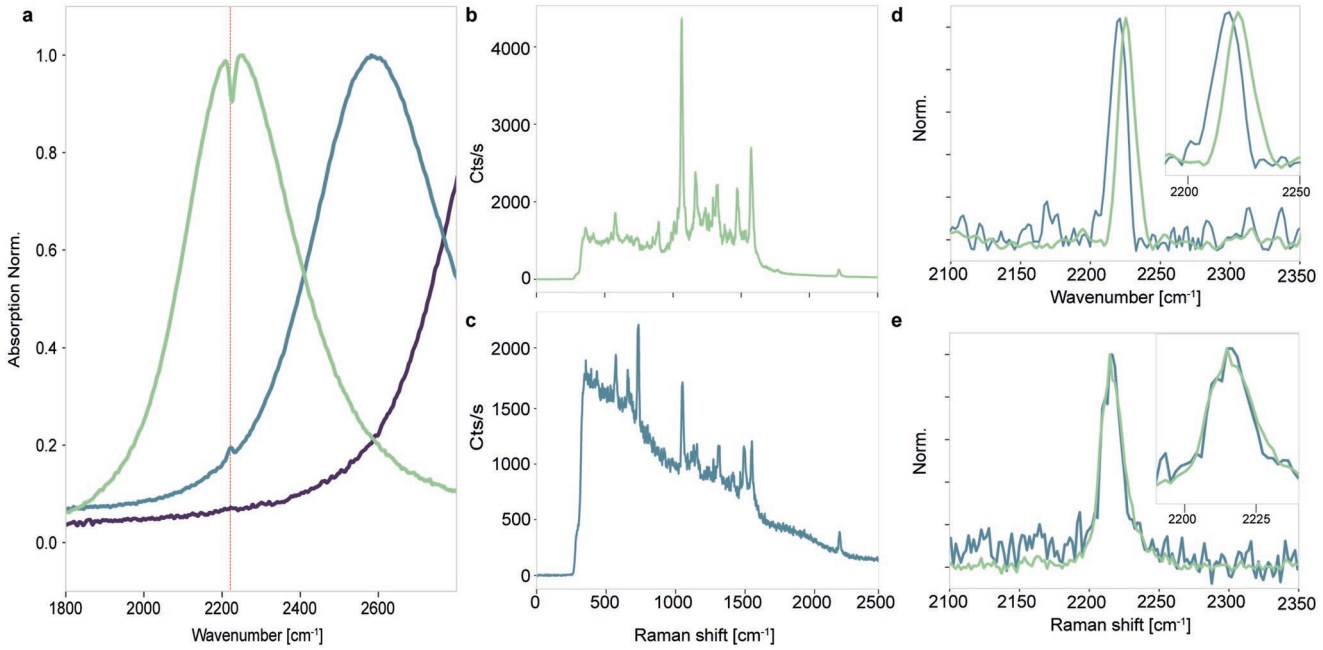

Figure 4. Complementary surface-enhanced vibrational spectroscopy of coupled and uncoupled 4-MBN self-assembled monolayers. a) Experimental FTIR microscopy spectra of three fields with varying degrees of detuning between the mid-IR resonant mode and the CN bond vibration (dashed red line). b,c). SERS spectra of NRoMs with mid-IR resonance frequencies that b) match or c) are detuned from the CN bond vibration frequency. d). Baseline-corrected SEIRAS of the matching (green) and detuned (blue) systems. Inset shows a zoomed-in view at the ≈5 cm^{-1} vibration shift between the two systems. e). SERS spectra of the matching (green) and detuned (blue) systems. Inset shows a zoomed-in look at the complete overlap between the two systems.

signal that scales as $|E(\omega)/E_0(\omega)|^2$ and the simulated field enhancement profiles, we set an upper bound for the SEIRAS enhancement at $\approx|230|^2 = 5.3 \times 10^4$.

2.4. Complementary SERS and SEIRAS of Coupled and Uncoupled SAMs

The ability to conduct complementary surface-enhanced vibrational spectroscopy on the same molecular population with SERS and SEIRAS presents an enticing opportunity to compare the vibrational information obtained with the two spectroscopies. Perhaps, an even more intriguing question is how the SERS and SEIRAS vibrational signatures change when comparing fields with different degrees of coupling (detuning) between the mid-IR optical mode and the CN bond vibration. Figure 4a shows FTIR spectra of 3 fields with different degrees of detuning. With a highly detuned (uncoupled) system, where there is no overlap between the mid-IR resonance and the CN bond vibration, the CN vibrational signal is too weak to be detected in our setup (purple). Therefore, we focus on a detuned system with enough overlap to detect the CN vibration signal (blue) and a frequency-matched system (green). Complementary SERS spectra of the frequency-matched (Figure 4b) and the detuned (Figure 4c) systems are subsequently collected (additional SERS spectra collected from NRoMs with varying degrees of detuning can be found in Figure S9, Supporting Information). In Figure 4d,e, we zoom in on the CN vibrations of the frequency-matched (green) and the detuned (blue) systems. In Figure 4d, we use the baseline-corrected SEIRAS curves, and in Figure 4e the complementary SERS spectra. Interestingly, while the matched system shows a clear ≈5 cm^{-1} blue shift compared to the detuned system (Figure 4d) when using background-subtracted SEIRAS, the CN vibrations of both systems gathered with SERS show overlapping signals with no apparent shift. To ensure that the observed shift in the baseline-corrected SEIRAS is not artificially generated during the correction routine, we have compared two approaches. One is a frequently used baseline-correction routine,[7,14,32] and the other is based on subtracting a reconstructed, non-perturbed resonance lineshape (details in Experimental Section). Using both approaches the ≈5 cm^{-1} difference between the matched and detuned system is clearly observed (Figure S10, Supporting Information). We have also employed a Fano lineshape correction scheme using a phase factor retrieval and found that the observed shifts remain after the correction scheme was employed (Figure S10, Supporting Information).[33]

Shifts in the vibration frequency of vibrationally coupled and uncoupled molecules can be expected according to perturbation theory,[34] however, the fact that this shift is only seen in the SEIRAS measurements is unsettling. Uncovering the origin of this discrepancy requires further investigation. These could include single NRoMs measurements both in SERS and SEIRAS. Given the large field enhancements of the VIS and mid-IR modes, it would likely be possible to explore very small molecular populations and ensure that the complementary information stems specifically from the same small population bound to the same cavity. Furthermore, the concentration of 4-MBN in the SAM can be adjusted by assembling a mixture of thiols. That way, the number of coupled CN bonds

could be varied and the impact of the molecular (CN bond) concentration on the observed shift could be determined providing insight into the origin of the observed frequency shift. Additionally, other bond vibrations should also be probed in frequency-matched and unmatched conditions to evaluate the generality of the phenomenon. The NRoM-based complementary approach seems an ideal platform to explore further this phenomenon.

Interestingly, a similar mismatch in the vibrational information observed with IR absorption and Raman scattering has recently been discussed in the context of chemistry under vibrational strong coupling (VSC).[35] In this emerging field, groundbreaking demonstrations of altered chemical processes under VSC conditions have generated great interest,[36–38] but some fundamental questions remain open.[39] One puzzling observation is the clear and straightforward detection of spectral splitting and coupled polaritonic states with IR absorption spectroscopy while in Raman spectra, only elusive to nonexistent detection of these coupled states has been observed.[40–43] One proposed reason for the absence of polaritonic features in the Raman spectra is that large numbers of uncoupled molecules co-exist with the coupled molecules and dominate the Raman spectra. NRoMs could offer a unique platform to probe specifically vibrationally coupled molecules through SERS, provided that VSC conditions can be reached in an optimized configuration. The NRoMs mid-IR resonances (long-axis) could be tuned to couple specific chemical bonds, while the vibrational signature of the same molecular population can be probed through SERS (short-axis, VIS resonances) without the need for IR photons (probing dark conditions). Typical Fabry-Pérot microcavities, on the other hand, do not support any Raman enhancement and their geometry often makes it more difficult to measure bulk Raman scattering.

This ability to conduct complementary investigations on the same molecular population with SERS and SEIRAS using NRoMs is especially interesting also for the upconversion of mid-IR light,[44,45] and for investigating plasmonic chemistry in a non-perturbative manner. In plasmon-mediated chemistry, reactions are driven by VIS plasmon resonances.[46] Using the same resonances to gather SERS spectra and track changes to the vibrational signature of reactants as the chemical reaction evolves is a beneficial and commonly used approach.[47] However, using the same plasmon resonances to drive chemistry and probe the system is a perturbative approach that often requires also relatively high laser powers. Furthermore, such SERS investigations are mostly confined to common laser lines (typically 532, 633, or 785 nm), limiting the ability to investigate chemical reactions driven by plasmonic resonances at frequencies that do not overlap with these laser lines. On the contrary, with NRoMs, the tunable short-axis gap plasmon resonances can be used to drive a chemical reaction in arbitrary frequencies while monitoring vibrational changes with SEIRAS through the long-axis mid-IR resonances.

3. Conclusion

In this work, we have demonstrated that NRoMs provide an advantageous platform for complementary surface-enhanced vibrational investigations. The VIS and mid-IR gap resonances of NRoMs support spatially overlapping and highly enhanced near-fields. The spatial overlap allows probing the same monolayer molecular population with SERS and SEIRAS, while the large field enhancements ensure strong surface-enhanced vibrational signals. Conveniently, the resonances in both spectral ranges can be easily tuned to match specific frequencies in high resolution. In this work, we match the VIS resonances with the laser frequency of our SERS setup and target CN bond vibrations with the mid-IR resonances. The relative ease of fabrication, reproducibility, and small size of NRoMs, along with the speed and simplicity of acquiring mid-IR spectra using a standard, commercial FTIR microscope, offer many advantages for SEIRAS applications. We demonstrate strong SERS and SEIRAS vibrational signals from a thiol monolayer and demonstrate the strength of the complementary surface-enhanced vibrational spectroscopy approach by highlighting differences in the vibrational signals obtained with the two methods when probing a vibrationally coupled system. We discuss the advantages of using NRoM nanocavities to explore cavity-modified chemistry, and highlight that our platform is ideally suited to explore why the spectral splitting under VSC conditions into lower and upper polaritons has been routinely observed using IR spectroscopy but has not been similarly seen in Raman spectra.

4. Experimental Section

Electromagnetic Simulations: 3D electromagnetic simulations using finite-difference time-domain (FDTD) software (Lumerical) to obtain the electric-field enhancement profiles in three dimensions, and the polarization-dependent extinction spectra for NRoMs with different widths and lengths are performed. More details can be found in the Supporting Information in the discussion following Figure S1 (Supporting Information).

NRoM Fabrication: Si substrates of 12 × 12 mm were cut from a 4 inch boron-doped <100> orientation single-crystal wafer (Siegert Wafer GmbH). The cut samples were sonicated for 10 min in acetone, isopropanol, and water followed by a mild oxygen plasma descumming (10 s, 50 W. Oxford instruments-Plasmalab 80+). i) Mirror substrates: On the cleaned Si substrates, a chromium adhesion layer (5 nm) and a thick gold layer (100 nm) were deposited (0.05 kÅ rate) in a Polyteknik E-Flex e-beam physical vapor deposition system. Then a home-built atomic layer deposition (ALD) system was used to deposit a thin (2–4 nm) Al_2O_3 spacer on the gold mirror. ii) Nanorod Arrays fabrication: On cleaned Si substrates, 1,1,1,3,3,3-Hexamethyldisilazane (HMDS-Primer, micro resist technology) was spin-coated on the samples (accelerated at 1000 rpm s^{-1} to 4000 rpm, and maintained for 35 s. Suss MicroTec-Delta 80 spin coater). The spin-coated samples were baked at 150 °C for 1 min. Next, CSAR AR-P 6200.13 (All Resist) was spin-coated (accelerated at 1000 rpm s^{-1} to 4000 rpm, and maintained for 45 s) followed by a 3 min bake at 150 °C to produce a ≈500 nm thick resist layer. Subsequently, this substrate was exposed to an e-beam with a dose of 200 μC cm^{-2} at 50 kV (Raith Voyager) to form arrays of rectangles 70 nm wide and with varying lengths (500–800 nm). After development (60 s in phentylacetate, 6 s in *o*-xylene, and 15 s in an MIBK:IPA 9:1 volume ratio solution) and a short descumming step, Seventy nanometer gold was deposited (0.05 kÅ rate) in a Polyteknik E-Flex e-beam physical vapor deposition system, followed by lift-off in Anisole at 65 °C. iii) NRoM formation: A thermal release sheet for electronic component processing (Nitto) was placed on the nanorod arrays, stripped and placed on the mirror substrate. The substrate was placed on a hotplate at 90 °C for ≈2 min until the thermal sheet

could be easily removed, leaving the nanorod arrays on the coated mirrors. Further details can be found in Section S2 of the Supporting Information.

Analyte Incorporation: The analyte was assembled onto the nanorods by soaking the NRoM sample in a 10 mM solution of 4-MBN in ethanol for ≈24 h to form a self-assembled monolayer.[48] Importantly. the 4-MBN molecules did not assemble onto the gold mirror since it was already coated with a thin Al_2O_3, layer. After the soaking period, the sample was placed in a clean ethanol solution for ≈5 min to remove any residual material and eventually dried with N_2. Two main protocols were tested to ensure that the 4-MBN monolayer was formed also in the gap between the nanorods and the coated mirrors where the field enhancement is maximal. Further details can be found in Section S6 of the Supporting Information.

Electron Microscopy: High-resolution scanning electron microscopy (SEM) images were acquired using an FEI Verios 460 with an acceleration voltage and current of 5 kV and 100 pA, respectively.

Fourier-Transform Infrared (FTIR) Microscope: A Bruker Hyperion coupled to a Bruker Vertex 80v spectrometer was used in reflection mode through a ×15 reflective objective. Nitrogen was continuously flown into a small home-built chamber around the microscope stage to minimize the CO_2 and H_2O vapors. In a typical measurement, FTIR spectra were obtained by collecting the signal from an NRoM array (typically integration times of 30–60 s) and correcting for the background signal collected from an adjacent bare mirror under the same collection conditions. Raw data can be found at https://doi.org/10.6084/m9.figshare.21586593.

Integrating Sphere Microscopy: A tunable light source (NKT FIU-15) was sent through an acousto-optic tunable filter (Crystal Technologies, approximately 5 nm bandwidth). The incident was sent through a polarizing beam splitter (Thorlabs) and a half wave-plate (Thorlabs) to control the polarization orientation. A long working distance objective (Mitutoyo M Apo Plan NIR ×50 NA 0.42 objective with a 17 mm working distance) was used to focus and collect light. The samples were mounted on a 3D piezoelectric stage (Piezojena Tritor400) positioned below a narrow slit of a modified GPS-020-SL integrating sphere (LabSphere). After positioning, the integrated spere was lowered so that the sample was positioned inside the sphere. For the measurements, low-noise Newport 818-UV calibrated photodiodes or Thorlabs PDA100A2 photodetectors, each connected to Stanford Research Systems SR830 lock-in amplifiers is used. The transmission of the acousto-optic tunable filter was digitally modulated as a source for the lock-in amplifiers. Extinction spectra were obtained by positioning a single NRoM in the focus spot center and scanning the incoming wavelengths (580–780 nm) with the acousto-optic tunable filter (typical measurements were done under ≈1.2–2.4 $\mu W\ \mu m^{-2}$ illumination). The collected signals were corrected with the reflection signal of a bare mirror in an adjacent location.

Raman Measurements: SERS experiments using a 772 nm wavelength were taken using a home-built confocal microscopy setup coupled to a spectrometer (Andor Shamrock A-SR-303i-B-SIL) with a cooled CCD camera (Andor iVac A-DR324B-FI). Excitation was performed with a narrowband tunable diode laser (Toptica DL-Pro 780) spectrally cleaned with a pair of bandpass filters (Semrock TBp01-790/12) and directed onto the sample by an Olympus objective (MPlan IR, 100×, NA = 0.95) that was also used for collection. The laser beam was filtered from the collected light with a pair of notch filters (Thorlabs NF785-33) allowing detection of both Stokes and anti-Stokes signals. Typical measurements were done under 360 $\mu W\ \mu m^{-2}$ excitation, 5–10 s collection time. The CN vibration ≈2200 cm^{-1}, the aromatic ring stretch ≈1600 cm^{-1}, and the C—CN stretch or CH in-plane deformation ≈1000 cm^{-1} were assigned according to previous reports.[49]

FTIR Background Correction: A baseline correction routine using an adaption of the computational approach of asymmetric least-squares smoothing (AsLSS) introduced by Eilers was used.[32] Alternatively, the resonance line shape was reconstructed by excluding data points around the interaction frequencies (≈2220 cm^{-1}) and fitting the line shape with multiple Voigt functions to minimize the residuals. Then the reconstructed line shape was subtracted from the FTIR raw data. When the resonance frequency of the nanocavity and the bond vibration frequency match, the background correction gives an inverted Lorentzian line shape. For convenience, the absolute value of the inverted Lorentzian was presented throughout the manuscript.

Supporting Information

Supporting Information is available from the Wiley Online Library or from the author.

Acknowledgements

This work was supported by the Dutch Research Council (NWO), project number OCENW.XS5.022. The authors also acknowledge support from the European Unions Horizon 2020 research and innovation program under Grant Agreement No. 829067 (FET Open THOR).

Conflict of Interest

The authors declare no conflict of interest.

Data Availability Statement

The data that support the findings of this study are available from the corresponding author upon reasonable request.

Keywords

nanocavity, nanophotonics, plasmonics, polaritonic chemistry, vibrational spectroscopy

Received: September 26, 2022
Revised: November 22, 2022
Published online:

[1] P. Larkin, *Infrared and Raman Spectroscopy* (Ed: P. Larkin), Elsevier, Oxford, UK **2011**, p. 1.
[2] F. Neubrech, C. Huck, K. Weber, A. Pucci, H. Giessen, *Chem. Rev.* **2017**, *117*, 5110.
[3] K. Maquelin, C. Kirschner, L. P. Choo-Smith, N. van den Braak, H. P. Endtz, D. Naumann, G. J. Puppels, *J Microbiol Methods* **2002**, *51*, 255.
[4] A. Sarycheva, Y. Gogotsi, *Chem. Mater.* **2020**, *32*, 3480.
[5] J.-B. Wu, M.-L. Lin, X. Cong, H.-N. Liu, P.-H. Tan, *Chem. Soc. Rev.* **2018**, *47*, 1822.
[6] X. Wang, S.-C. Huang, S. Hu, S. Yan, B. Ren, *Nat Rev Phys* **2020**, *2*, 253.
[7] L. Kühner, M. Hentschel, U. Zschieschang, H. Klauk, J. Vogt, C. Huck, H. Giessen, F. Neubrech, *ACS Sens.* **2017**, *2*, 655.
[8] M. Fleischmann, P. J. Hendra, A. J. McQuillan, *Chem. Phys. Lett.* **1974**, *26*, 163.
[9] D. L. Jeanmaire, R. P. Van Duyne, *J. Electroanal. Chem. Interfacial Electrochem.* **1977**, *84*, 1.
[10] A. Hartstein, J. R. Kirtley, J. C. Tsang, *Phys. Rev. Lett.* **1980**, *45*, 201.
[11] H.-L. Wang, E.-M. You, R. Panneerselvam, S.-Y. Ding, Z.-Q. Tian, *Light Sci Appl* **2021**, *10*, 161.

[12] L. Dong, X. Yang, C. Zhang, B. Cerjan, L. Zhou, M. L. Tseng, Y. Zhang, A. Alabastri, P. Nordlander, N. J. Halas, *Nano Lett.* **2017**, *17*, 5768.
[13] J. J. Baumberg, J. Aizpurua, M. H. Mikkelsen, D. R. Smith, *Nat. Mater.* **2019**, *18*, 668.
[14] C. Huck, F. Neubrech, J. Vogt, A. Toma, D. Gerbert, J. Katzmann, T. Härtling, A. Pucci, *ACS Nano* **2014**, *8*, 4908.
[15] X. Chen, C. Ciracì, D. R. Smith, S.-H. Oh, *Nano Lett.* **2015**, *15*, 107.
[16] E. Oksenberg, I. Shlesinger, A. Xomalis, A. Baldi, J. J. Baumberg, A. F. Koenderink, E. C. Garnett, *Nat. Nanotechnol.* **2021**, *16*, 1378.
[17] A. Rose, T. B. Hoang, F. McGuire, J. J. Mock, C. Ciracì, D. R. Smith, M. H. Mikkelsen, *Nano Lett.* **2014**, *14*, 4797.
[18] R. Chikkaraddy, B. de Nijs, F. Benz, S. J. Barrow, O. A. Scherman, E. Rosta, A. Demetriadou, P. Fox, O. Hess, J. J. Baumberg, *Nature* **2016**, *535*, 127.
[19] F. Neubrech, A. Pucci, T. W. Cornelius, S. Karim, A. García-Etxarri, J. Aizpurua, *Phys. Rev. Lett.* **2008**, *101*, 157403.
[20] K. Chen, R. Adato, H. Altug, *ACS Nano* **2012**, *6*, 7998.
[21] B. Cerjan, X. Yang, P. Nordlander, N. J. Halas, *ACS Photonics* **2016**, *3*, 354.
[22] H. Wang, J. Kundu, N. J. Halas, *Angew. Chem., Int. Ed.* **2007**, *46*, 9040.
[23] F. Le, D. W. Brandl, Y. A. Urzhumov, H. Wang, J. Kundu, N. J. Halas, J. Aizpurua, P. Nordlander, *ACS Nano* **2008**, *2*, 707.
[24] C. D'Andrea, J. Bochterle, A. Toma, C. Huck, F. Neubrech, E. Messina, B. Fazio, O. M. Maragò, E. Di Fabrizio, M. Lamy de La Chapelle, P. G. Gucciardi, A. Pucci, *ACS Nano* **2013**, *7*, 3522.
[25] N. S. Mueller, E. Pfitzner, Y. Okamura, G. Gordeev, P. Kusch, H. Lange, J. Heberle, F. Schulz, S. Reich, *ACS Nano* **2021**, *15*, 5523.
[26] H. Agrawal, E. C. Garnett, *Nanocube Imprint Lithography ACS Nano* **2020**, *14*, 11009.
[27] F. J. García de Abajo, *Rev. Mod. Phys.* **2007**, *79*, 1267.
[28] M. F. Limonov, M. V. Rybin, A. N. Poddubny, Y. S. Kivshar, *Nat. Photonics* **2017**, *11*, 543.
[29] X. Wu, S. K. Gray, M. Pelton, *Nanoscale Plasmonic Resonator Opt. Express* **2010**, *18*, 23633.
[30] H. Hinterwirth, S. Kappel, T. Waitz, T. Prohaska, W. Lindner, M. Lämmerhofer, *ACS Nano* **2013**, *7*, 1129.
[31] D. Dregely, F. Neubrech, H. Duan, R. Vogelgesang, H. Giessen, *Nat. Commun.* **2013**, *4*, 2237.
[32] P. H. C. Eilers, *Anal. Chem.* **2003**, *75*, 3631.
[33] G. Tek, P. Hamm, *J. Phys. Chem. Lett.* **2020**, *11*, 6185.
[34] P. Lalanne, W. Yan, K. Vynck, C. Sauvan, J.-P. Hugonin, *Laser Photonics Rev.* **2018**, *12*, 1700113.
[35] K. Nagarajan, A. Thomas, T. W. Ebbesen, *J. Am. Chem. Soc.* **2021**, *143*, 16877.
[36] A. Thomas, L. Lethuillier-Karl, K. Nagarajan, R. M. A. Vergauwe, J. George, T. Chervy, A. Shalabney, E. Devaux, C. Genet, J. Moran, T. W. Ebbesen, *Science* **2019**, *363*, 615.
[37] J. Lather, P. Bhatt, A. Thomas, T. W. Ebbesen, J. George, *Angew. Chem., Int. Ed.* **2019**, *58*, 10635.
[38] A. Thomas, J. George, A. Shalabney, M. Dryzhakov, S. J. Varma, J. Moran, T. Chervy, X. Zhong, E. Devaux, C. Genet, J. A. Hutchison, T. W. Ebbesen, *Angew. Chem., Int. Ed.* **2016**, *55*, 11462.
[39] D. S. Wang, S. F. Yelin, *ACS Photonics* **2021**, *8*, 2818.
[40] W. M. Takele, L. Piatkowski, F. Wackenhut, S. Gawinkowski, A. J. Meixner, J. Waluk, *Phys. Chem. Chem. Phys.* **2021**, *23*, 16837.
[41] W. Ahn, B. S. Simpkins, *J. Phys. Chem. C* **2021**, *125*, 830.
[42] K. S. Menghrajani, M. Chen, K. Dholakia, W. L. Barnes, *Adv. Opt. Mater.* **2022**, *10*, 2102065.
[43] F. Verdelli, J. J. P. M. Schulpen, A. Baldi, J. G. Rivas, *J. Phys. Chem. C* **2022**, *126*, 7143.
[44] W. Chen, P. Roelli, H. Hu, S. Verlekar, S. P. Amirtharaj, A. I. Barreda, T. J. Kippenberg, M. Kovylina, E. Verhagen, A. Martínez, C. Galland, *Science* **2021**, *374*, 1264.
[45] A. Xomalis, X. Zheng, R. Chikkaraddy, Z. Koczor-Benda, E. Miele, E. Rosta, G. A. E. Vandenbosch, A. Martínez, J. J. Baumberg, *Science* **2021**, *374*, 1268.
[46] C. Zhan, M. Moskovits, Z.-Q. Tian, *Matter* **2020**, *3*, 42.
[47] C. Boerigter, R. Campana, M. Morabito, S. Linic, *Nat. Commun.* **2016**, *7*, 10545.
[48] S. Gal, J. Salewski, D. Millo, I. Zebger, S. Franzen, P. Hildebrandt, *Int. J. Mol. Sci.* **2012**, *13*, 7466.
[49] H. Rudolf, *J. Solid State Electrochem.* **2013**, *17*, 1869.